Supporting Tables, Figures, and Discussion for:

In Situ Characterization of Waters of Hydration in a Variable-Hydrate Active Pharmaceutical Ingredient using ^{35}Cl Solid-State NMR and X-ray Diffraction

David A. Hirsh,[1,†] Sean T. Holmes,[2] Paroma Chakravarty,[3] Austin A. Peach,[2] Antonio G. DiPasquale,[3] Karthik Nagapudi,[3,*] and Robert W. Schurko[2,*]

[1] *Department of Chemistry & Biochemistry, University of Windsor, Windsor, ON, N9B 3P4, Canada*
[2] *Department of Chemistry & Biochemistry, Florida State University, Tallahassee, FL, 32308*
[3] *Department of Small Molecule Pharmaceutical Sciences, Genentech, Inc., South San Francisco, CA, 94080*
[†] *Current address: Boehringer Ingelheim Pharmaceuticals, Inc., Ridgefield, CT 06877*

* Authors to whom correspondence should be addressed:
R.W.S. Phone: 850-645-8614; E-mail: rschurko@fsu.edu
K.N. Phone: 650-452-2548 E-mail: nagapudi.karthik@gene.com

Supporting Information Provided:

Table S1. Composition of tablets produced by dry or wet granulation.

Component	Dry Granulated Tablet		Wet Granulated Tablet	
	% w/w	weight (mg)	% w/w	weight (mg)
Intragranular				
GDC-0927 HCl Salt	58.7	567.5	58.7	567.5
Microcrystalline Cellulose, Avicel PH101	35.1 (QS)	286.4	34.3 (QS)	263.6
Hydroxypropyl Cellulose, Klucel EXF	0.0	0.0	3.0	23.0
Croscarmellose Sodium (Ac-Di-Sol® SD-711)	2.0	16.3	0.0	0.0
Fumed Silica (Aerosil 200 Pharma)	1.0	8.2	0.0	0.0
Magnesium Stearate, Hyqual® 2257	0.625	5.1	0.0	0.0
Purified Water	0.0	0.0	25-30	QS
Extragranular				
Croscarmellose Sodium (Ac-Di-Sol® SD-711)	2.0	16.3	3.0	23.0
Magnesium Stearate, Hyqual® 2257	0.625	5.1	1.0	7.7
Core	100	967.5	100	967.5
Opadry II Brown 85F165010 or 85F165037	3.0	29.0	3.0	29.0
Total		996.5		996.5

Table S2. Crystal data and structure refinement for **GNE-A**.

X-ray ID	GNE-A	
Sample/notebook ID	G02950761.23-1	
Empirical formula	C56 H62 Cl2 F2 N2 O10	
Formula weight	1031.97	
Temperature	100(2) K	
Wavelength	1.54178 Å	
Crystal system	Monoclinic	
Space group	P 21	
Unit cell dimensions	*a* = 16.0884(6) Å	α= 90°
	b = 9.7370(4) Å	β= 114.967(3)°
	c = 17.8444(7) Å	γ = 90°
Volume	2534.15(18) $Å^3$	
Z	2	
Density (calculated)	1.352 mg/m^3	
Absorption coefficient	1.731 mm^{-1}	
F(000)	1088	
Crystal size	0.040 x 0.030 x 0.030 mm^3	
Theta range for data collection	2.731 to 68.612°.	
Index ranges	-19<=h<=19, -11<=k<=10, -21<=l<=21	
Reflections collected	58893	
Independent reflections	9022 [R(int) = 0.0489]	
Completeness to theta = 67.000°	99.9 %	
Absorption correction	Semi-empirical from equivalents	
Max. and min. transmission	0.929 and 0.753	
Refinement method	Full-matrix least-squares on F^2	
Data / restraints / parameters	9022 / 1 / 677	
Goodness-of-fit on F^2	1.042	
Final R indices [I>2sigma(I)]	R1 = 0.0753, wR2 = 0.2170	
R indices (all data)	R1 = 0.0837, wR2 = 0.2282	
Absolute structure parameter	0.081(8)	
Extinction coefficient	n/a	
Largest diff. peak and hole	0.914 and -1.185 $e.Å^{-3}$	

Table S3. Atomic coordinates ($\times 10^4$) and equivalent isotropic displacement parameters ($Å^2 \times 10^3$) for **GNE-A**. U_{eq} is defined as one third of the trace of the orthogonalized U_{ij} tensor.

	x	y	z	U_{eq}
C(1)	9377(4)	7986(7)	4277(4)	36(1)
C(2)	8632(4)	8432(7)	3463(4)	33(1)
C(3)	7760(4)	7992(7)	3216(4)	33(1)
C(4)	7561(4)	7012(7)	3744(4)	34(1)
C(5)	6727(4)	6315(7)	3495(4)	38(1)
C(6)	6567(4)	5389(8)	3988(4)	40(2)
C(7)	7249(5)	5104(9)	4772(4)	44(2)
C(8)	8091(5)	5773(9)	5039(4)	43(2)
C(9)	8236(4)	6721(7)	4541(4)	36(1)
C(10)	8947(4)	9254(7)	2925(4)	36(1)
C(11)	9527(5)	10393(7)	3227(5)	42(2)
C(12)	9829(5)	11114(8)	2707(5)	44(2)
C(13)	9573(5)	10708(8)	1899(5)	45(2)
C(14)	9007(4)	9584(7)	1599(5)	41(2)
C(15)	8707(4)	8853(7)	2107(4)	37(1)
C(16)	6983(4)	8410(7)	2424(4)	37(1)
C(17)	10021(4)	6922(7)	4195(4)	32(1)
C(18)	10919(4)	6853(8)	4760(4)	40(2)
C(19)	11517(4)	5867(8)	4707(4)	40(2)
C(20)	11212(4)	4931(8)	4071(4)	37(1)
C(21)	10301(5)	4980(8)	3490(4)	41(1)
C(22)	9716(4)	5939(7)	3552(4)	36(1)
C(23)	12687(4)	3909(9)	4452(4)	42(2)
C(24)	13127(5)	2897(9)	4082(5)	47(2)
C(25)	13534(6)	2628(10)	2836(5)	56(2)
C(26)	12775(6)	3218(11)	2010(6)	61(2)
C(27)	12236(6)	3541(10)	2523(5)	54(2)
C(28)	12399(9)	2287(11)	1310(7)	77(3)
C(29)	5573(4)	3059(7)	838(4)	37(1)
C(30)	6541(4)	3241(7)	1524(4)	33(1)
C(31)	6729(4)	2644(7)	2267(4)	35(1)
C(32)	6039(4)	1756(7)	2338(4)	38(1)
C(33)	6078(5)	1295(8)	3094(4)	43(2)
C(34)	5449(5)	380(8)	3133(5)	46(2)
C(35)	4745(5)	-149(8)	2392(5)	48(2)
C(36)	4696(4)	316(8)	1646(4)	42(2)
C(37)	5304(5)	1277(7)	1606(4)	39(2)
C(38)	7160(4)	4119(7)	1324(4)	36(1)
C(39)	6837(4)	5308(8)	844(4)	38(2)
C(40)	7407(5)	6091(7)	626(4)	42(2)
C(41)	8324(5)	5724(8)	862(4)	40(1)
C(42)	8643(4)	4539(7)	1318(4)	39(1)
C(43)	8088(4)	3760(8)	1561(4)	38(1)

C(44)	7595(5)	2892(8)	3024(4)	42(2)
C(45)	4904(4)	4131(7)	869(4)	35(1)
C(46)	4154(4)	4487(8)	151(4)	40(2)
C(47)	3532(5)	5484(8)	171(5)	45(2)
C(48)	3660(5)	6094(8)	906(5)	43(2)
C(49)	4391(5)	5725(9)	1629(5)	47(2)
C(50)	5003(5)	4753(8)	1603(5)	45(2)
C(51)	2277(6)	7372(11)	306(5)	59(2)
C(52)	1740(6)	8341(10)	585(6)	58(2)
C(53)	855(5)	8359(10)	1494(5)	51(2)
C(54)	1389(9)	7664(13)	2389(9)	43(2)
C(54A)	1583(14)	8500(20)	2331(12)	43(2)
C(55)	2222(6)	7642(12)	2116(5)	62(2)
C(56)	1509(10)	8521(16)	3122(9)	49(3)
C(56A)	1355(15)	7590(30)	2877(13)	49(5)
N(1)	13104(4)	3452(7)	3304(4)	43(1)
N(2)	1522(4)	7662(6)	1228(3)	38(1)
O(1)	9031(3)	7472(6)	4860(3)	42(1)
O(2)	8706(3)	9105(6)	783(3)	46(1)
O(3)	5719(3)	4757(6)	3692(4)	51(1)
O(4)	11741(3)	3941(6)	3934(3)	41(1)
O(5)	5232(3)	1688(5)	855(3)	39(1)
O(6)	9518(3)	4061(6)	1542(3)	42(1)
O(7)	5531(4)	9(7)	3904(4)	59(1)
O(8)	3098(3)	7088(6)	1001(4)	50(1)
O(9)	14051(4)	5837(7)	3510(4)	61(2)
O(10)	5526(8)	2593(9)	4599(7)	124(4)
F(1)	12088(7)	1074(7)	1556(5)	106(3)
F(2)	1827(6)	9827(8)	3035(5)	60(2)
F(2A)	1132(15)	6305(15)	2481(10)	85(6)
Cl(1)	527(1)	5006(2)	480(1)	53(1)
Cl(2)	3799(2)	-1116(3)	3818(2)	80(1)

Table S4. Anisotropic displacement parameters ($Å^2 x\ 10^3$)for **GNE-A**. The anisotropic displacement factor exponent takes the form: $-2\pi^2[\ h^2 a^{*2} U^{11} + ... + 2\ h\ k\ a^*\ b^*\ U^{12}\ ]$.

	U^{11}	U^{22}	U^{33}	U^{23}	U^{13}	U^{12}
C(1)	32(3)	37(4)	41(3)	-9(3)	18(3)	-3(3)
C(2)	28(3)	30(3)	41(3)	-11(2)	14(2)	-3(2)
C(3)	31(3)	32(3)	36(3)	-8(2)	16(2)	4(2)
C(4)	31(3)	35(3)	36(3)	-9(2)	15(2)	2(2)
C(5)	32(3)	42(4)	41(3)	0(3)	19(3)	4(3)
C(6)	34(3)	43(4)	47(4)	-7(3)	21(3)	-1(3)
C(7)	41(3)	51(4)	47(4)	5(3)	27(3)	5(3)
C(8)	35(3)	56(5)	37(3)	-2(3)	16(3)	6(3)
C(9)	32(3)	45(4)	35(3)	-7(3)	18(3)	1(3)
C(10)	29(3)	28(3)	50(4)	0(3)	16(3)	4(2)
C(11)	35(3)	36(4)	53(4)	-10(3)	16(3)	0(3)
C(12)	34(3)	31(4)	64(4)	-7(3)	17(3)	-1(3)
C(13)	43(4)	29(4)	61(4)	9(3)	20(3)	6(3)
C(14)	31(3)	37(4)	51(4)	3(3)	14(3)	3(3)
C(15)	34(3)	31(3)	45(3)	2(3)	17(3)	4(3)
C(16)	32(3)	35(3)	44(3)	0(3)	17(3)	4(3)
C(17)	29(3)	36(3)	32(3)	-3(2)	13(2)	-2(2)
C(18)	34(3)	51(4)	31(3)	-9(3)	9(2)	-6(3)
C(19)	26(3)	57(4)	32(3)	0(3)	8(2)	3(3)
C(20)	34(3)	43(4)	35(3)	3(3)	16(2)	4(3)
C(21)	39(3)	44(4)	35(3)	-7(3)	11(3)	2(3)
C(22)	35(3)	30(3)	38(3)	-4(3)	9(2)	2(3)
C(23)	33(3)	53(4)	38(3)	11(3)	15(3)	8(3)
C(24)	41(3)	47(4)	58(4)	13(3)	24(3)	10(3)
C(25)	52(4)	58(5)	70(5)	-10(4)	38(4)	3(4)
C(26)	57(5)	69(6)	60(5)	10(4)	28(4)	0(4)
C(27)	50(4)	67(6)	45(4)	-3(4)	22(3)	5(4)
C(28)	113(9)	56(6)	83(7)	1(5)	61(7)	10(6)
C(29)	34(3)	47(4)	29(3)	-4(3)	13(3)	5(3)
C(30)	33(3)	37(3)	27(3)	-4(2)	12(2)	8(2)
C(31)	31(3)	39(4)	35(3)	-6(3)	13(3)	9(3)
C(32)	37(3)	38(4)	38(3)	0(3)	16(3)	10(3)
C(33)	41(3)	45(4)	39(3)	2(3)	13(3)	13(3)
C(34)	46(4)	48(4)	48(4)	8(3)	23(3)	13(3)
C(35)	46(4)	40(4)	69(5)	5(3)	34(4)	11(3)
C(36)	32(3)	46(4)	46(4)	2(3)	14(3)	12(3)
C(37)	39(3)	38(4)	42(3)	0(3)	18(3)	11(3)
C(38)	36(3)	40(4)	29(3)	-7(3)	11(2)	7(3)
C(39)	36(3)	45(4)	31(3)	-3(3)	12(2)	10(3)
C(40)	52(4)	34(4)	38(3)	-3(3)	17(3)	8(3)
C(41)	44(3)	38(4)	40(3)	-8(3)	20(3)	-4(3)
C(42)	35(3)	42(4)	36(3)	-10(3)	13(3)	1(3)
C(43)	39(3)	40(4)	34(3)	-2(3)	15(3)	6(3)
C(44)	35(3)	53(4)	35(3)	-1(3)	11(3)	9(3)
C(45)	34(3)	35(4)	33(3)	1(2)	11(2)	3(3)
C(46)	29(3)	48(4)	39(3)	8(3)	11(3)	0(3)
C(47)	33(3)	45(4)	53(4)	21(3)	15(3)	9(3)
C(48)	39(3)	39(4)	54(4)	7(3)	23(3)	6(3)
C(49)	46(4)	48(4)	46(4)	-3(3)	18(3)	14(3)
C(50)	42(3)	48(5)	40(4)	-4(3)	12(3)	13(3)
C(51)	54(4)	80(6)	53(4)	29(4)	32(4)	26(4)
C(52)	46(4)	65(6)	75(5)	34(5)	38(4)	23(4)

C(53)	31(3)	67(5)	54(4)	-11(4)	17(3)	3(3)
C(54)	55(6)	36(6)	55(6)	1(5)	39(5)	-4(5)
C(54A)	55(6)	36(6)	55(6)	1(5)	39(5)	-4(5)
C(55)	50(4)	84(7)	46(4)	-14(4)	14(4)	26(4)
C(56)	64(8)	43(8)	53(7)	-4(6)	35(6)	1(6)
C(56A)	59(12)	56(16)	37(10)	0(10)	24(9)	-10(10)
N(1)	40(3)	51(4)	45(3)	3(3)	25(3)	9(3)
N(2)	33(3)	39(3)	44(3)	0(2)	19(2)	-1(2)
O(1)	35(2)	57(3)	36(2)	-12(2)	16(2)	-7(2)
O(2)	48(3)	50(3)	42(2)	5(2)	22(2)	-1(2)
O(3)	39(2)	54(4)	62(3)	4(3)	22(2)	-8(2)
O(4)	34(2)	50(3)	38(2)	3(2)	14(2)	11(2)
O(5)	44(2)	39(3)	34(2)	-6(2)	16(2)	2(2)
O(6)	37(2)	46(3)	45(3)	-4(2)	19(2)	-1(2)
O(7)	63(3)	65(4)	55(3)	19(3)	30(3)	13(3)
O(8)	36(2)	47(3)	64(3)	3(2)	18(2)	8(2)
O(9)	50(3)	54(4)	79(4)	4(3)	27(3)	0(3)
O(10)	189(10)	68(5)	206(10)	-74(6)	172(9)	-75(6)
F(1)	161(7)	50(4)	96(5)	-8(3)	44(5)	-14(4)
F(2)	86(6)	42(4)	63(5)	-13(3)	42(4)	-9(4)
F(2A)	158(17)	49(8)	76(9)	-5(7)	78(11)	-30(9)
Cl(1)	57(1)	50(1)	67(1)	-17(1)	40(1)	-14(1)
Cl(2)	88(2)	86(2)	70(1)	-5(1)	38(1)	-17(1)

Table S5. Hydrogen coordinates ($\times 10^4$) and isotropic displacement parameters ($Å^2 \times 10^3$) for **GNE-A**.

	x	y	z	U(eq)
H(1)	9755	8818	4534	43
H(5)	6256	6495	2962	45
H(7)	7141	4460	5121	52
H(8)	8565	5571	5568	51
H(11)	9715	10677	3785	51
H(12)	10215	11892	2915	53
H(13)	9784	11198	1553	54
H(15)	8331	8066	1894	44
H(16A)	7157	9228	2204	55
H(16B)	6443	8618	2526	55
H(16C)	6838	7659	2023	55
H(18)	11139	7497	5201	48
H(19)	12135	5840	5110	48
H(21)	10086	4340	3047	49
H(22)	9093	5946	3158	44
H(23A)	12791	3614	5016	50
H(23B)	12958	4833	4488	50
H(24A)	13769	2726	4478	57
H(24B)	12792	2013	3972	57
H(25A)	13499	1621	2895	67
H(25B)	14164	2918	2946	67
H(26)	12992	4085	1849	73
H(27A)	11955	4467	2417	65
H(27B)	11778	2831	2480	65
H(28A)	11882	2734	848	93
H(28B)	12875	2052	1117	93
H(29)	5615	3169	298	44

H(33)	6552	1623	3593	51
H(35)	4319	-807	2413	58
H(36)	4233	-35	1147	51
H(39)	6215	5573	667	46
H(40)	7175	6900	309	50
H(41)	8716	6275	711	48
H(43)	8331	2968	1892	45
H(44A)	7979	2066	3152	63
H(44B)	7447	3108	3490	63
H(44C)	7927	3664	2926	63
H(46)	4060	4058	-357	48
H(47)	3022	5736	-325	54
H(49)	4473	6134	2139	57
H(50)	5507	4501	2103	54
H(51A)	1927	6516	89	71
H(51B)	2409	7799	-135	71
H(52A)	2102	9184	814	70
H(52B)	1166	8604	108	70
H(53A)	214	8042	1193	61
H(53B)	891	9374	1500	61
H(54)	1156	6722	2417	52
H(54A)	1787	9453	2533	52
H(55A)	2616	8470	2284	75
H(55B)	2595	6793	2276	75
H(56A)	917	8607	3164	59
H(56B)	1956	8079	3634	59
H(56C)	1885	7509	3422	59
H(56D)	829	7968	2961	59
H(2)	1309	6703	1048	45
H(2)	9021	9467	563	68
H(3)	5764	4009	3941	77
H(6)	9781	4542	1316	64
H(7A)	5124	-569	3856	89
H(9X)	14610	5632	3648	73
H(9Y)	13762	5096	3485	73
H(10X)	6067	2739	4963	149
H(10Y)	5506	1775	4426	149
H(2A)	4214	-1545	4538	96

Table S6. Acquisition parameters for $^{35}Cl\{^{1}H\}$ WURST-CPMG experiments (B_0 = 9.4 T).

	All Samples
Number of scans	44056
Experimental time (h)	6.12
Recycle delay (s)	0.5
Spectral Width (MHz)	1
^{35}Cl WURST pulse width (μs)	25
^{35}Cl WURST pulse rf (kHz)	19
^{1}H decoupling field (kHz)	62
Sweep range of WURST pulses (kHz)	500
Points in WURST shape [N]	500
Meiboom-Gill loops [N] (*i.e.*, Number of echoes)	44
Length of echoes (μs)	100
Acquisition length (number of points)	16700

Table S7. Acquisition parameters for $^{35}Cl\{^{1}H\}$ quadrupolar-echo experiments (B_0 = 21.1 T).

	All Samples
Number of scans	16384
Experimental time (h)	9.1
Recycle delay (s)	2
Spectral Width (kHz)	250
^{35}Cl pulse width (μs)	4
^{35}Cl pulse rf (kHz)	32
Inter-pulse delay [τ] (μs)	50
^{1}H decoupling field (kHz)	80
Acquisition length (number of points)	1024

Table S8. Acquisition parameters for ^{1}H-^{13}C CP/MAS (ν_{rot} = 12 kHz) experiments.

	As Received	All Other Samples
Number of scans	789	1248
Experimental time (hrs)	1.1	1.73
Recycle delay (s)	5	5
^{1}H 90° pulse width [π/2] (μs)	2.5	2.5
Contact time (ms)	1.5	1.5
^{1}H rf field during contact pulse (kHz)	40	40
^{13}C rf field during contact pulse (kHz)	51	51
^{1}H decoupling field (kHz)	47	47
Spectral width (kHz)	59.5	59.5
Acquisition length (number of points)	4096	4096

Table S9. Acquisition parameters for $^{2}H\{^{1}H\}$ quadrupolar-echo experiments.

	All Samples
Number of scans	201-600
Experimental time (min)[b]	120-15
Recycle delay (s)[c]	30-1
^{2}H 90° pulse width [π/2] (μs)	2.4
Inter-pulse delay [τ] (μs)	24
^{2}H rf field (kHz)	101
^{1}H decoupling field (kHz)	50
Spectral width (MHz)	1
Acquisition length (# of points)	2008

[a]The experimental time varied due to differences in the optimal recycle delay and number of scans acquired. [b]The recycle delay was optimized at each sample temperature. The optimal value progressively decreased as the sample was heated.

Table S10. Acquisition parameters for ^{1}H MAS Hahn echo experiments.

	All Samples	
Number of scans	16	48
Experimental time (min)	2.7	4
Recycle delay (s)	10	5
^{1}H 90° pulse width [π/2] (μs)	2.5	2.083
Inter-pulse delay [τ] (μs)	83.3	16.67
^{1}H 180° pulse width [π] (μs)	5	4.166
^{1}H rf field (kHz)	100	120
Spectral width (kHz)	150	33.33
Acquisition length (# of points)	1024	1024
MAS Rate (kHz)	12	60

Table S11. Acquisition parameters for ^{19}F UFMAS (ν_{rot} = 60 kHz) Hahn echo experiments.

	As Received
Number of scans	800
Experimental time (min)	67
Recycle delay (s)	5
^{19}F 90° pulse width [π/2] (μs)	2.083
Inter-pulse delay [τ] (μs)	16.67
^{19}F 180° pulse width [π] (μs)	4.166
^{19}F rf field (kHz)	120
Spectral width (kHz)	740
Acquisition length (# of points)	4090

Table S12. Close H···Cl⁻ contacts for the two crystallographically distinct Cl sites in three model dehydrates of GNE-A, as measured from the DFT-D2* optimized crystal structures.

Material	Conformer	Cl1†		Cl2†	
		Contact Type	Contact Distance (Å)	Contact Type	Contact Distance (Å)
α-GNE-A	A	$R_3NH^+\cdots Cl^-$	2.053	$HOH\cdots Cl^-$	2.154
		$ROH\cdots Cl^-$	2.213	$ROH\cdots Cl^-$	2.181
		$ROH\cdots Cl^-$	2.224	$ROH\cdots Cl^-$	2.198
	B	$R_3NH^+\cdots Cl^-$	2.171	$HOH\cdots Cl^-$	2.166
		$ROH\cdots Cl^-$	2.280	$ROH\cdots Cl^-$	2.166
		$ROH\cdots Cl^-$	2.281	$ROH\cdots Cl^-$	2.185
β-GNE-A	A	$R_3NH^+\cdots Cl^-$	2.049	$HOH\cdots Cl^-$	2.142
		$ROH\cdots Cl^-$	2.245	$R_3NH^+\cdots Cl^-$	2.143
		$ROH\cdots Cl^-$	2.313	$ROH\cdots Cl^-$	2.398
	B	$R_3NH^+\cdots Cl^-$	2.120	$R_3NH^+\cdots Cl^-$	2.148
		$ROH\cdots Cl^-$	2.375	$ROH\cdots Cl^-$	2.153
		$ROH\cdots Cl^-$	2.408	$ROH\cdots Cl^-$	2.408
γ-GNE-A	A	$R_3NH^+\cdots Cl^-$	2.048	$R_3NH^+\cdots Cl^-$	2.196
		$ROH\cdots Cl^-$	2.293	$ROH\cdots Cl^-$	2.292
		$ROH\cdots Cl^-$	2.329	$ROH\cdots Cl^-$	2.690
	B	$R_3NH^+\cdots Cl^-$	2.165	$R_3NH^+\cdots Cl^-$	2.190
		$ROH\cdots Cl^-$	2.423	$ROH\cdots Cl^-$	2.252
		$ROH\cdots Cl^-$	2.430	$ROH\cdots Cl^-$	2.417

Table S13. Enthalpies of dehydration for the three model dehydrates of GNE-A

Material	Conformer	H (eV)	ΔH_{deh} (kJ mol^{-1})
H_2O	-	-473.221	-
GNE-A	A	-8496.663	-
α-GNE-A	A	-8259.848	19.8
β-GNE-A	A	-8259.808	23.6
γ-GNE-A	A	-8022.875	54.8
GNE-A	B	-8496.664	-
α-GNE-A	B	-8259.816	22.9
β-GNE-A	B	-8259.743	29.9
γ-GNE-A	B	-8022.891	53.2

Table S14. Thermodynamic data used to assess the Boltzmann populations of conformers A and B of the model dehydrates of **GNE-A**.

Material	Conformer	H (eV)	ΔH_{con} (kJ mol^{-1})	exp[ΔH_{con} (kJ mol^{-1})]	Weight
α-GNE-A	A	-8259.848	0.0	1.000	0.77
	B	-8259.816	3.0	0.295	0.23
β-GNE-A	A	-8259.808	0.0	1.000	0.93
	B	-8259.743	6.2	0.081	0.07
γ-GNE-A	A	-8022.875	1.6	0.522	0.34
	B	-8022.891	0.0	1.000	0.66

Additional discussion of CASTEP calculations

The assignment of overlapping ^{35}Cl powder patterns in an ultra-wideline NMR spectrum to distinct Cl^- sites can be difficult without *a priori* knowledge of the ^{35}Cl EFG and CS tensors parameters associated with each site.[1] When a crystal structure is accurately known, NMR tensor parameters can be calculated with great accuracy using plane-wave DFT methods. In cases where the structure is poorly refined (*e.g.*, due to inaccurate hydrogen atom positions) or even unknown, it is possible to utilize plane-wave DFT methods to improve the refinement and/or solve the structure, a method known as *NMR crystallography*.[2–4] Recently, our group has developed a dispersion-corrected plane-wave density functional theory (DFT) method for the refinement of atomic coordinates determined by experimental diffraction methods via an empirical parameterization of Grimme's two-body dispersion force field.[5] This method, known as DFT-D2*, yields ^{35}Cl EFG tensors that are in excellent agreement with experimentally determined values, and has been demonstrated to optimize the positions of hydrogen atoms involved in hydrogen bonding with a precision rivaling that of neutron diffraction.

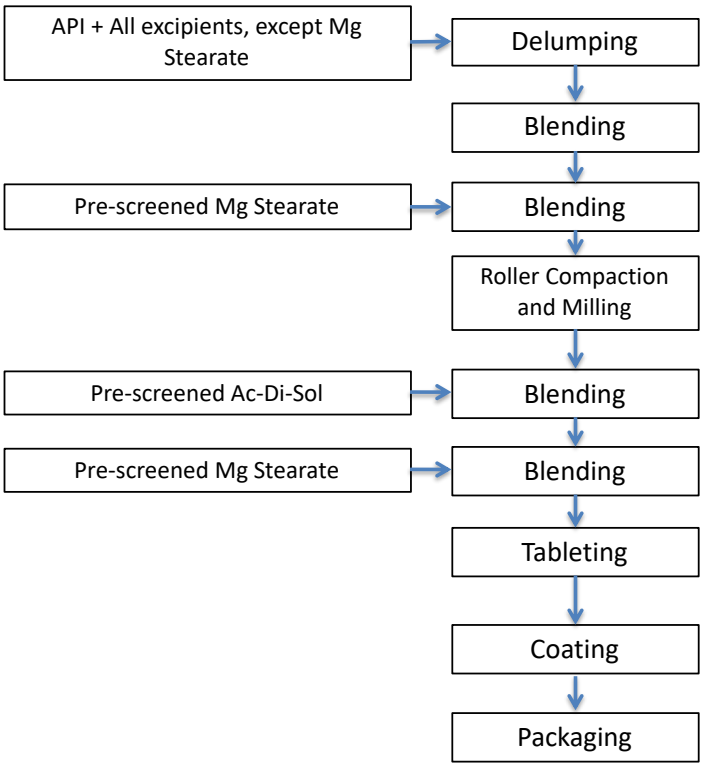

Figure S1. Dry granulation process scheme.

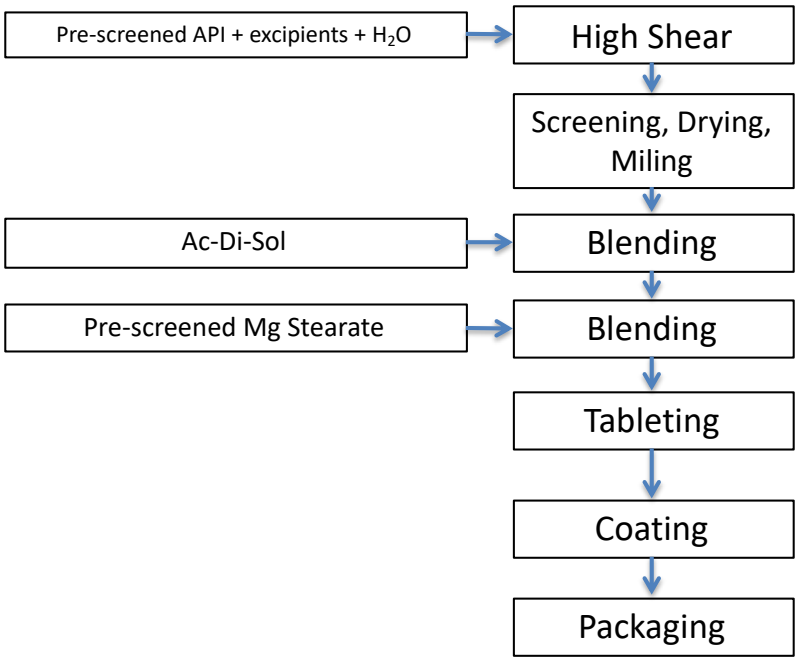

Figure S2. Wet granulation process scheme.

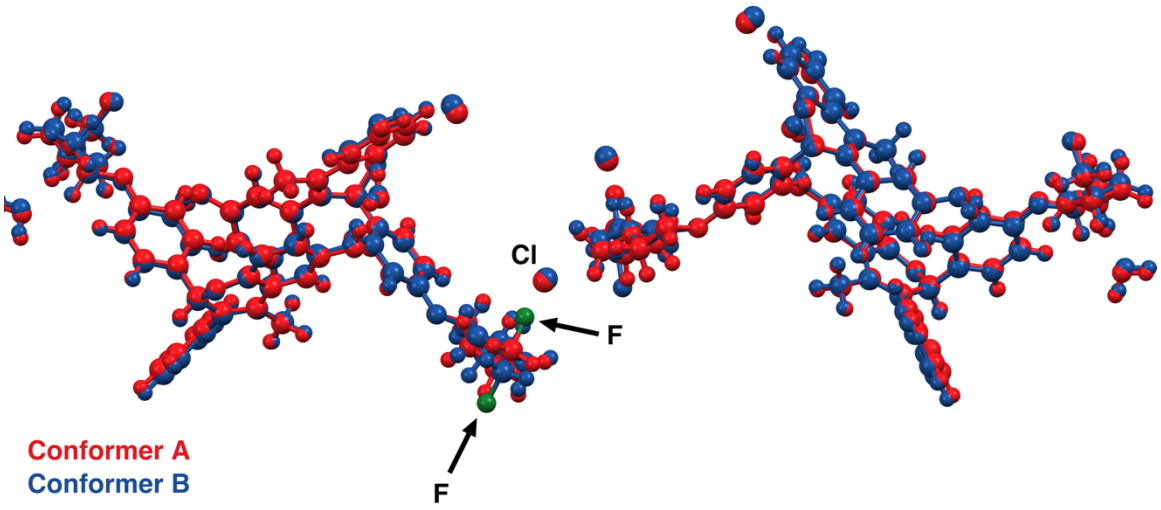

Figure S3. Overlay of the structures of the two GNE-A conformers Conformer A (red) and Conformer B (blue). The F atom (green) points either toward (Conformer A) or away from (Conformer B) the labeled Cl atom. See text for details.

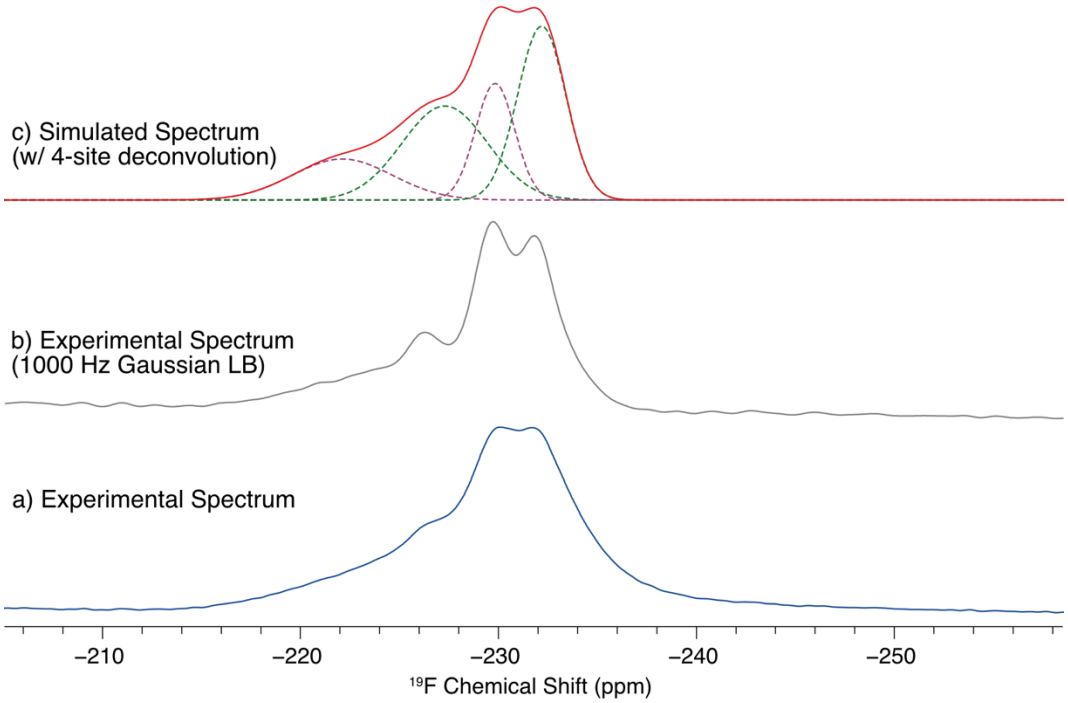

Figure S4. Experimental ^{19}F UFMAS (ν_{rot} = 60 kHz) spectra of **GNE-A** processed a) without line broadening and b) with 1 kHz Gaussian line broadening (which enhances the resolution of the ^{19}F signal and reveals at least 4 distinct features). A simulated spectrum is shown in c) with the deconvoluted peaks and combined pattern shown as dashed and solid lines, respectively. The dashed lines in the deconvolution are colored according to possible peak assignments to the two crystallographically-distinct ^{19}F sites in the conformers.

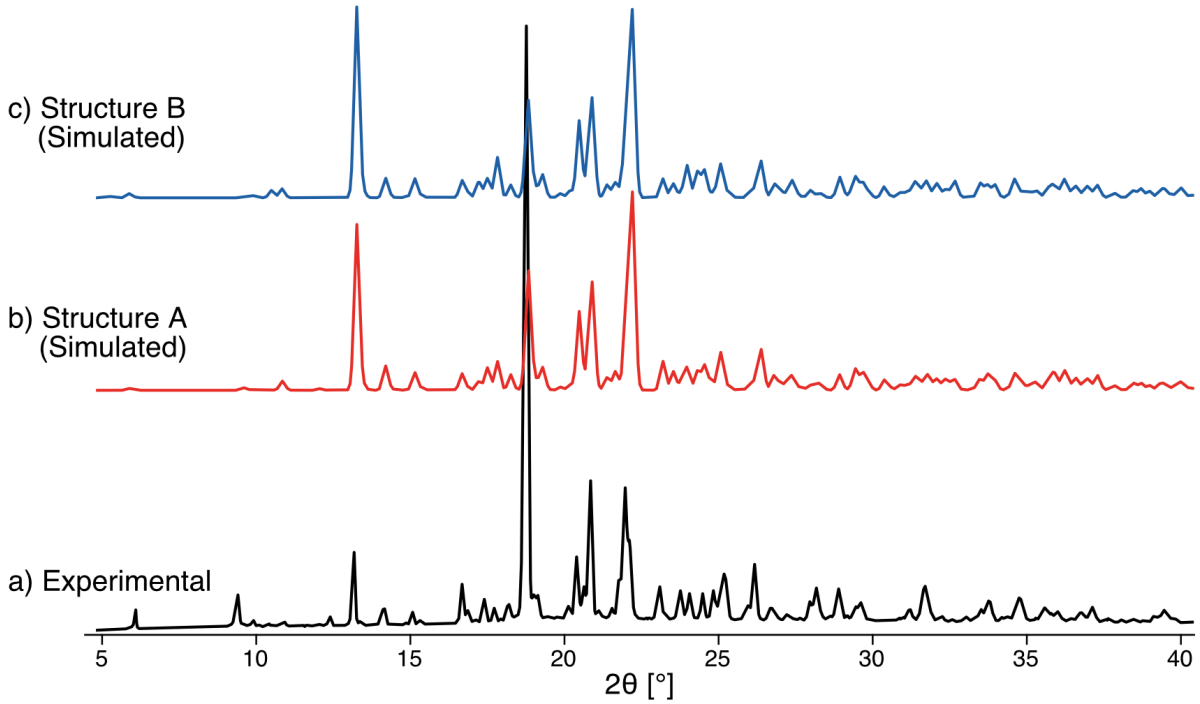

Figure S5. PXRD diffraction patterns of **GNE-A^{AR}** a) obtained experimentally at 298 K or simulated from the crystal structures of the two conformers b) **Conformer A**, and c) **Conformer B** acquired at 100 K. Slight discrepancies in the peak positions result from unit cell contraction at the low temperature.

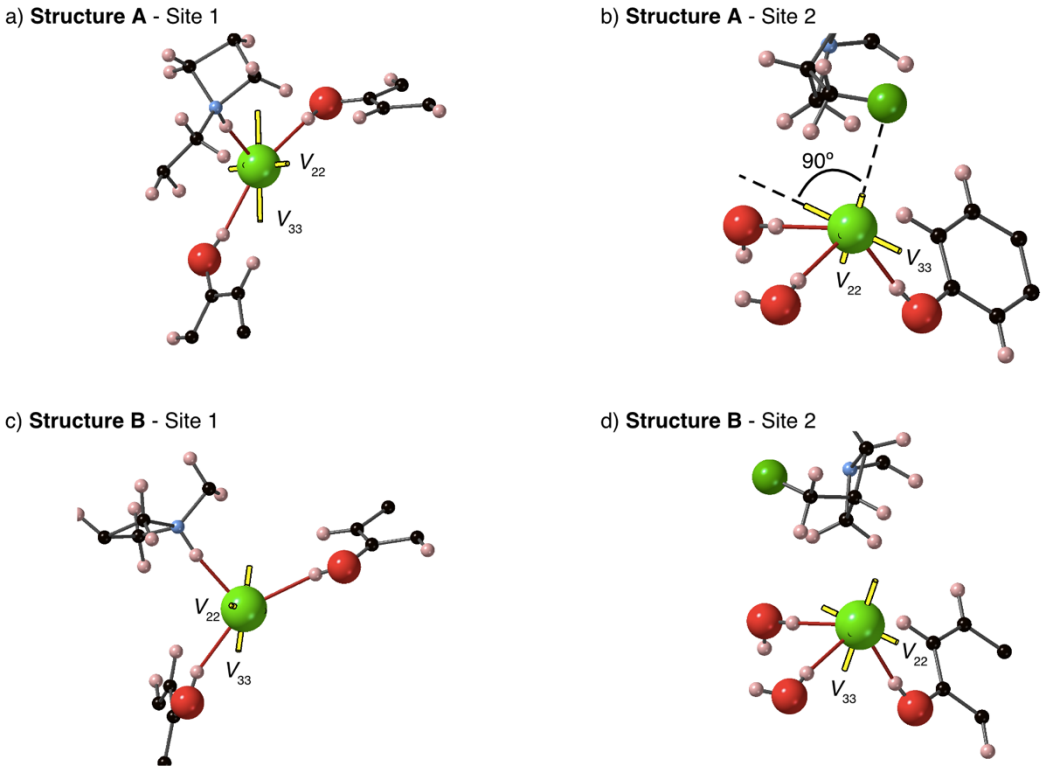

Figure S6. ^{35}Cl EFG tensor orientations in **GNE-A** calculated using CASTEP. The top row shows the two Cl^- environments in **Conformer A**, the bottom shows the corresponding environments in **Conformer B**. In b), the dashed lines indicate the orientations of V_{33} and the Cl···F contact, respectively. See text below for details.

Discussion of Figure S6

The large differences in the values of C_Q for Cl1 and Cl2 arise from differences in the three short H···Cl contacts that are *ca*. 2.2 Å or less; for instance, Cl1 features H···Cl interactions with one R_3N–H and two RO–H groups (in particular, the short R_3N-H contact of 2.034 Å likely accounts for the larger C_Q), whereas Cl2 has H···Cl interactions with one RO–H group and two H_2O molecules. The smaller variations in the quadrupolar parameters between **Conformers A** and **B** for both Cl1 and Cl2 are observed due to minor differences in H···Cl distances (for Cl1) and differences in the proximity of the CH_2F···Cl contacts (for Cl2). For Cl1, the large difference in C_Q between conformers A and B, 6.78 MHz and 5.57 MHz, can be explained by the differences in the short R_3N–H···Cl contacts of 2.034 Å and 2.090 Å, respectively, since it is well

established that a single, short H···Cl contact is most often the dominant influence on the chlorine EFG tensor parameters and orientation.[1] The orientation of V_{33} in these two conformers is similar (**Figure S6**). For Cl2, here is a change in sign of C_Q between conformers A and B, which very likely arises due to interactions between the F site in the CH_2F group and the nearest Cl^- ion. In **Conformer A**, the C-F bond is oriented towards the neighboring Cl^- site (F···Cl distance of 3.76 Å); but, in **Conformer B**, the C-F bond points away from the Cl^- site (F···Cl distance of 4.38 Å), apparently having a lesser effect on the ^{35}Cl EFG tensor parameters. In **Conformer A**, the largest component of the EFG tensor, V_{33}, is oriented perpendicular to the direction of the Cl···F contact, whereas in **Conformer B**, V_{33} is directed towards the water molecules (*i.e.*, it is not strongly influenced by the F atom). *N.B.*, It is not possible to determine the sign of C_Q from the experimental NMR spectra, but only its magnitude.

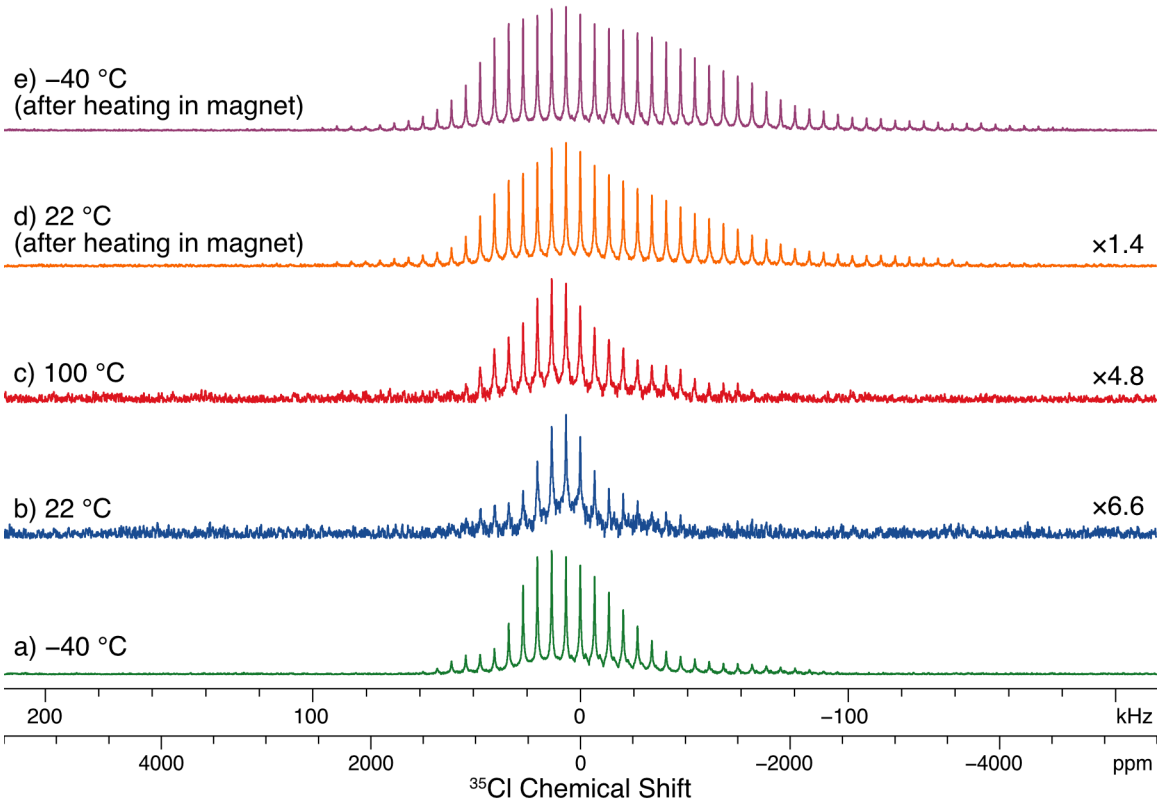

Figure S7. Variable-temperature $^{35}Cl\{^{1}H\}$ WURST-CPMG NMR spectra of **GNE-A** acquired under static sample conditions. The spectra are presented in the order in which they were acquired starting at a) −40 °C before heating and ending with e) −40 °C after heating. Spectra are vertically scaled to have the same maximum intensity (the scaling factors are shown on the right).

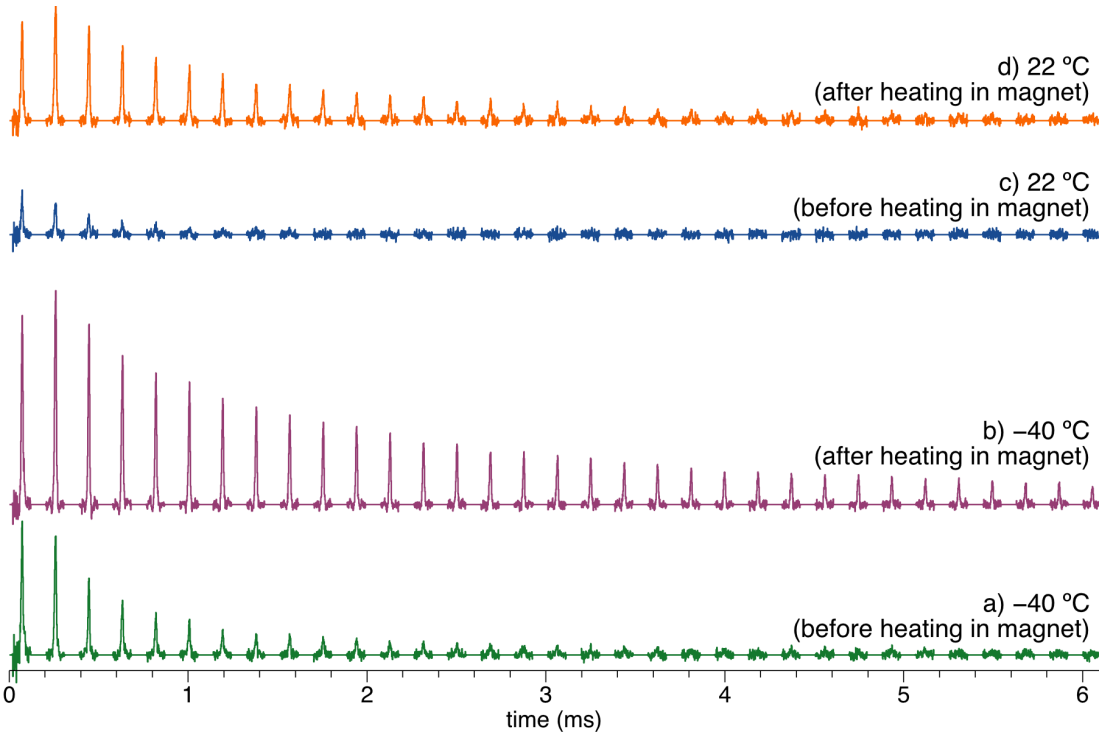

Figure S8. Experimental $^{35}Cl\{^{1}H\}$ WURST-CPMG echo trains of **GNE-A** acquired at −40 °C or 22 °C, before or after the samples were heated in the magnet (as indicated in the figure). $T_2^{eff}(^{35}Cl)$ values measured from these data are shown in **Table 3**.

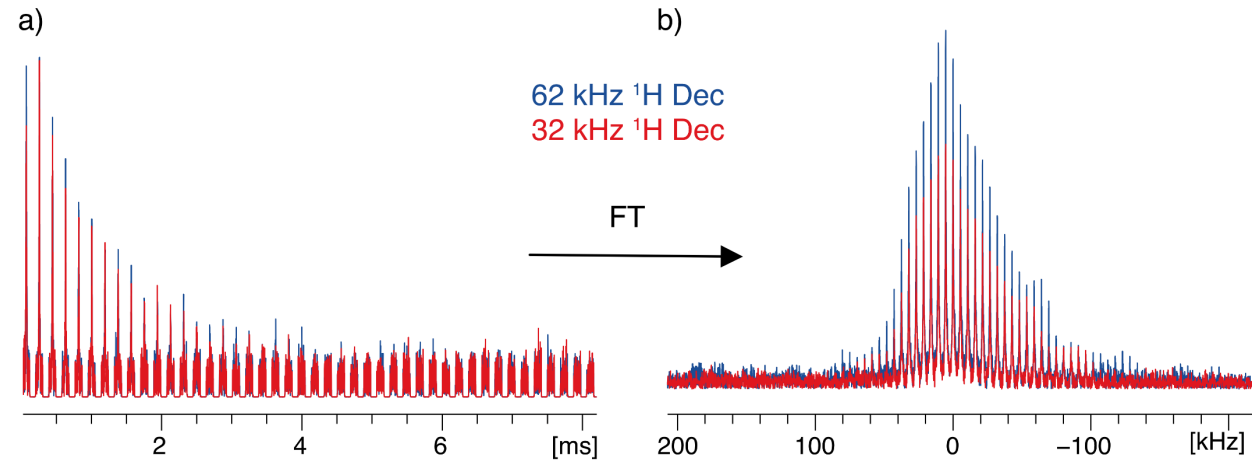

Figure S9. a) Experimental $^{35}Cl\{^{1}H\}$ WURST-CPMG echo trains of **GNE-A^{AR}** acquired with either 32 kHz (red) or 62 kHz (blue) ^{1}H decoupling. b) shows the Fourier transforms of the two echo trains.

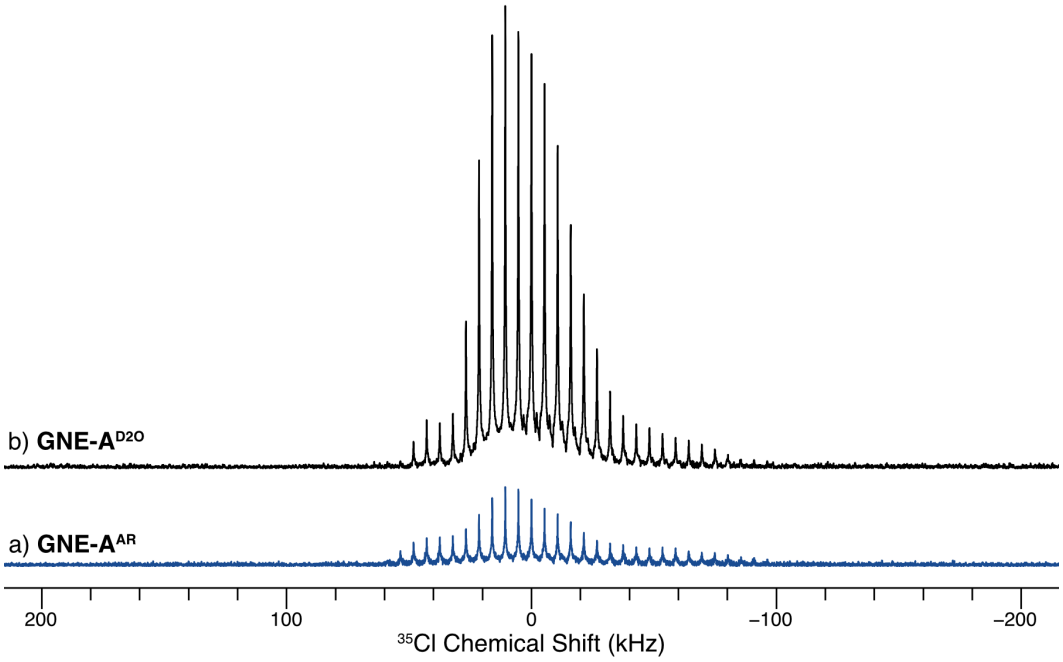

Figure S10. Experimental $^{35}Cl\{^{1}H\}$ WURST-CPMG NMR spectra of a) **GNE-A^{AR}** and b) after being dried and then rehydrated in a hydration chamber with D_2O (**GNE-A^{D2O}**). Spectra were acquired at −40 ºC.

Discussion of Figure S9 and Figure S10

As the $T_2^{eff}(^{35}Cl)$ is strongly dependent upon the magnitudes of the dipolar couplings between ^{35}Cl and proximate ^{1}H nuclei, changes in the ^{1}H decoupling strength or the substitution of deuterated H_2O (*i.e.*, D_2O) should have a substantial effect on ^{35}Cl spectra acquired with CPMG methods (*i.e.*, since ^{2}H-^{35}Cl dipolar couplings are smaller than ^{1}H-^{35}Cl couplings by a factor of 0.154, the $T_2^{eff}(^{35}Cl)$ should be substantially longer for a system in which ^{1}H are replaced by ^{2}H, and the signal in the corresponding ^{35}Cl CPMG spectra should be more intense). Indeed, a significant increase in ^{35}Cl signal intensity is seen in WURST-CPMG SSNMR spectra acquired with increased decoupling power (**Figure S9**).

To further confirm this point, an additional sample of **GNE-A** was prepared using the same drying and rehydration procedure used to make the **GNE-A^{LR}** sample, but using a rehydration chamber saturated with D_2O (this sample is referred to as **GNE-A^{D2O}**). As shown in

Figure S10, the addition of D_2O produces a large increase in the ^{35}Cl NMR signal intensity from the dihydrated Cl2 site with respect to that of the analogous non-deuterated sample. However, the signal corresponding to Cl1, does not change noticeably between the two samples. Such a substantial change in the ^{35}Cl NMR spectrum with deuteration is consistent with the D_2O incorporating into the structure. Finally, the fact that a pattern corresponding to Cl2′ is not observed in the ^{35}Cl NMR spectrum of **GNE-A^{D2O}**, suggests that is Cl2′ produced by the dehydration of the material, *and is not* a site that is present in **GNE-A^{AR}** that is observed due to an extremely short $T_2^{eff}(^{35}Cl)$.

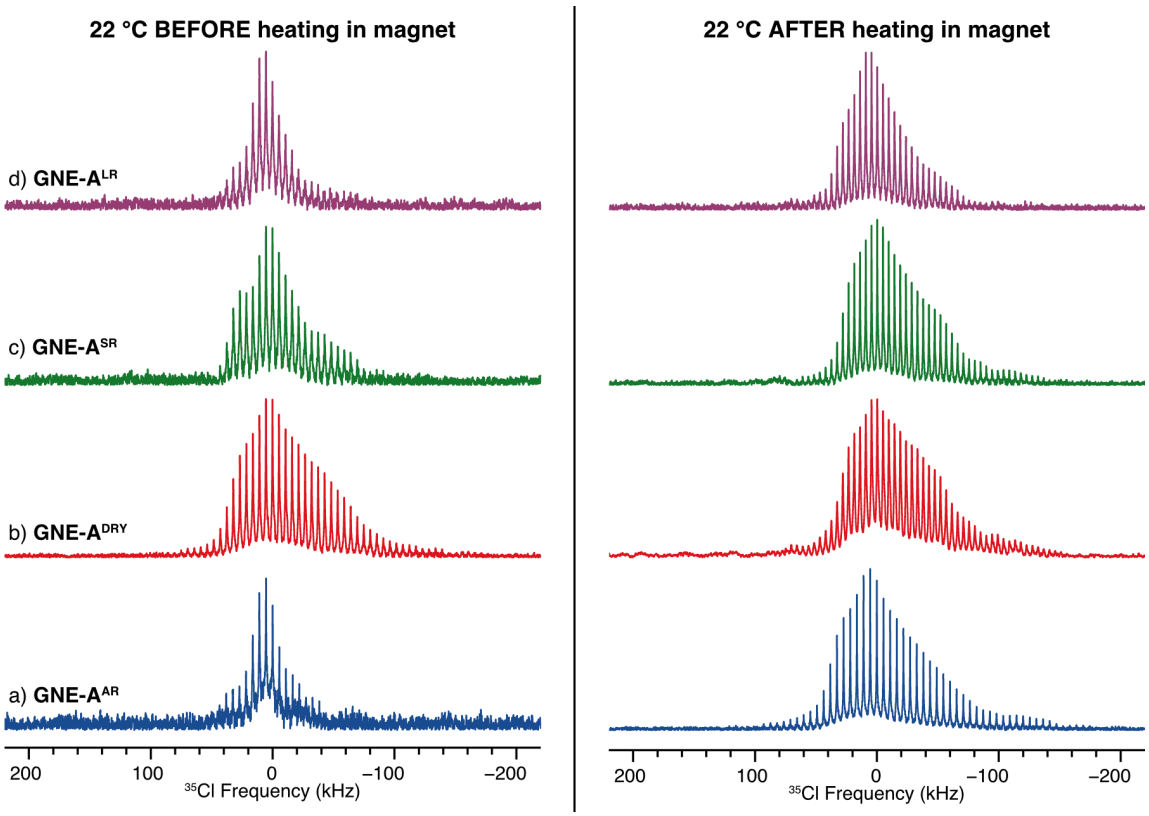

Figure S11. Experimental $^{35}Cl\{^{1}H\}$ WURST-CPMG NMR spectra of the four **GNE-A** samples acquired at 22 ºC before (left column) and after (right column) heating in the magnet.

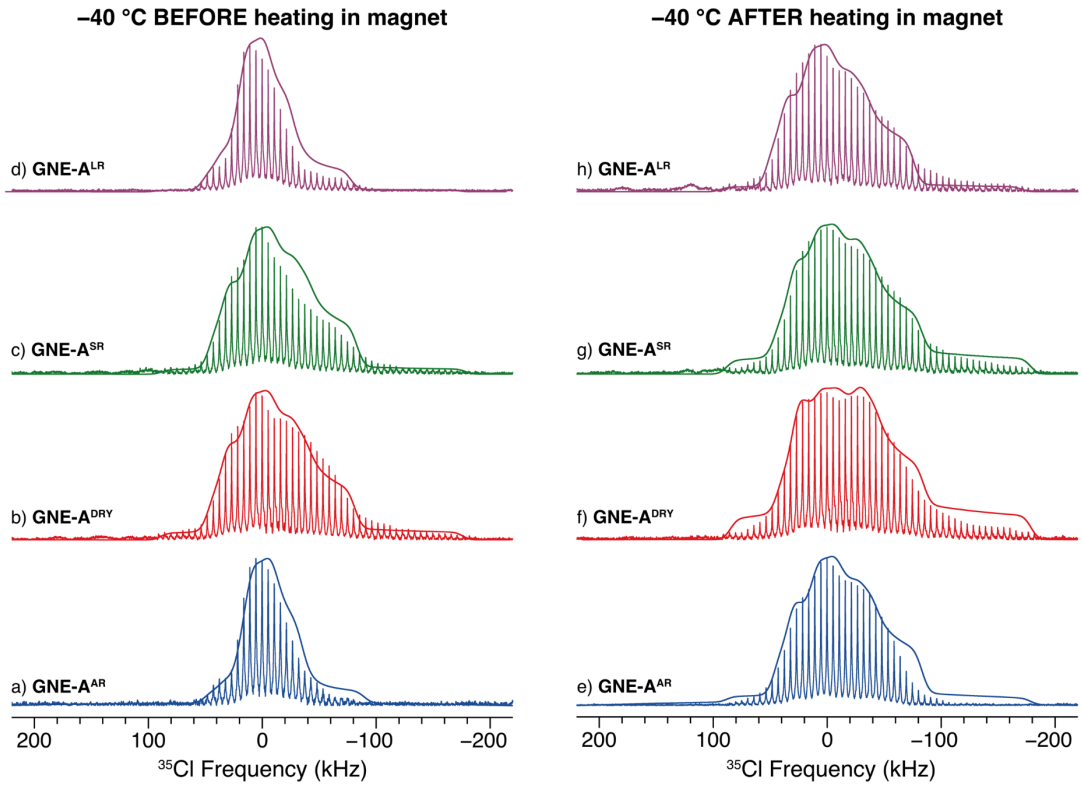

Figure S12. Experimental $^{35}Cl\{^{1}H\}$ WURST-CPMG NMR spectra of the four **GNE-A** samples acquired at −40 ºC before (left) and after (right) heating in the magnet. This figure is identical to **Figure 5**, except that the deconvoluted spectra are not shown.

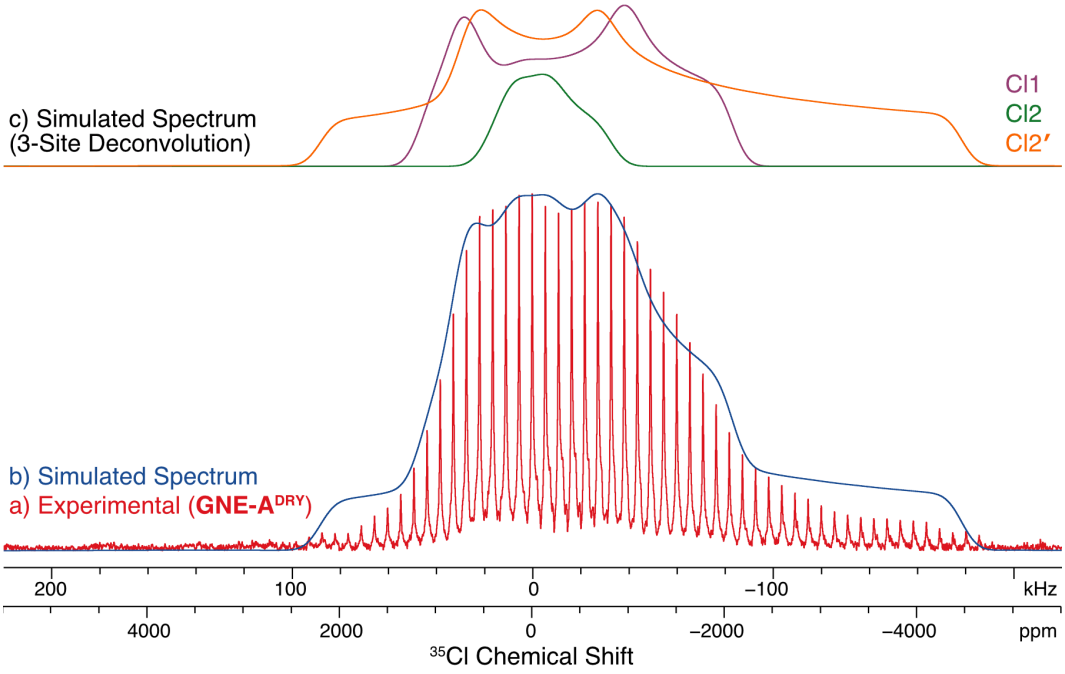

Figure S13. a) Experimental $^{35}Cl\{^{1}H\}$ WURST-CPMG NMR spectrum of the **GNE-A^{DRY}** sample, acquired at −40 ºC after heating in the magnet, b) analytical simulation of the pattern constructed from the 3 subspectra shown in c).

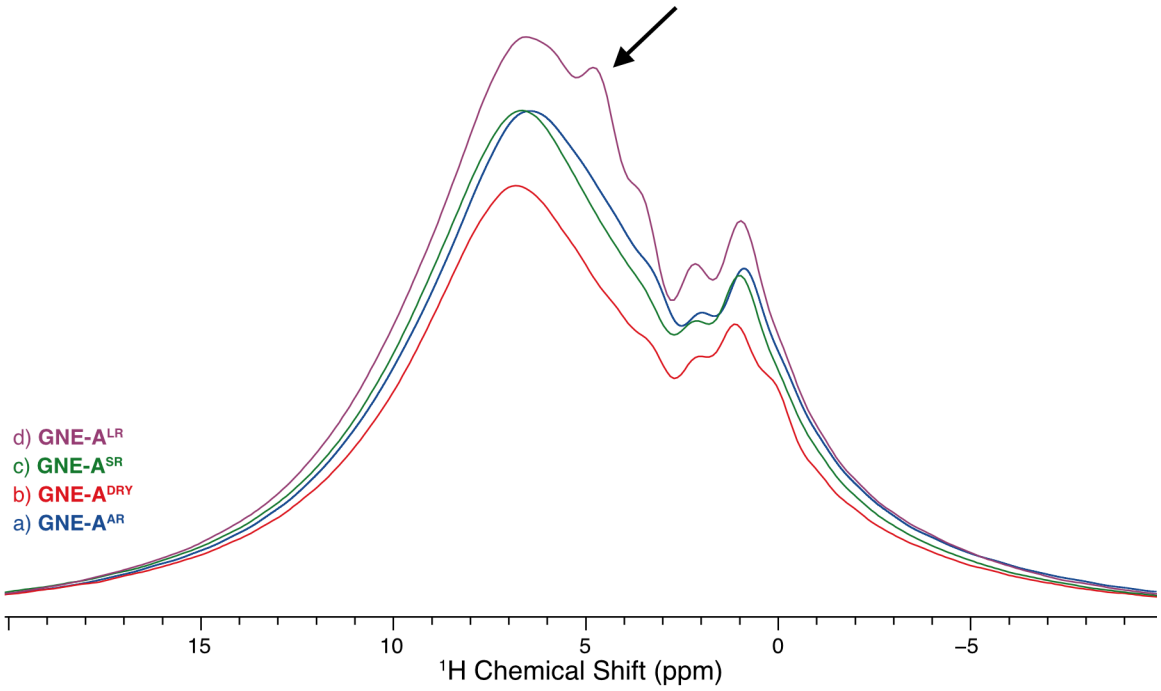

Figure S14. ^{1}H MAS (ν_{rot} = 12 kHz) NMR spectra of the **GNE-A** samples prepared with different levels of hydration. See text for details of the sample preparations. The arrow indicates the position of a distinct feature in the spectrum of **Rehydrate Long** that is mentioned in the text.

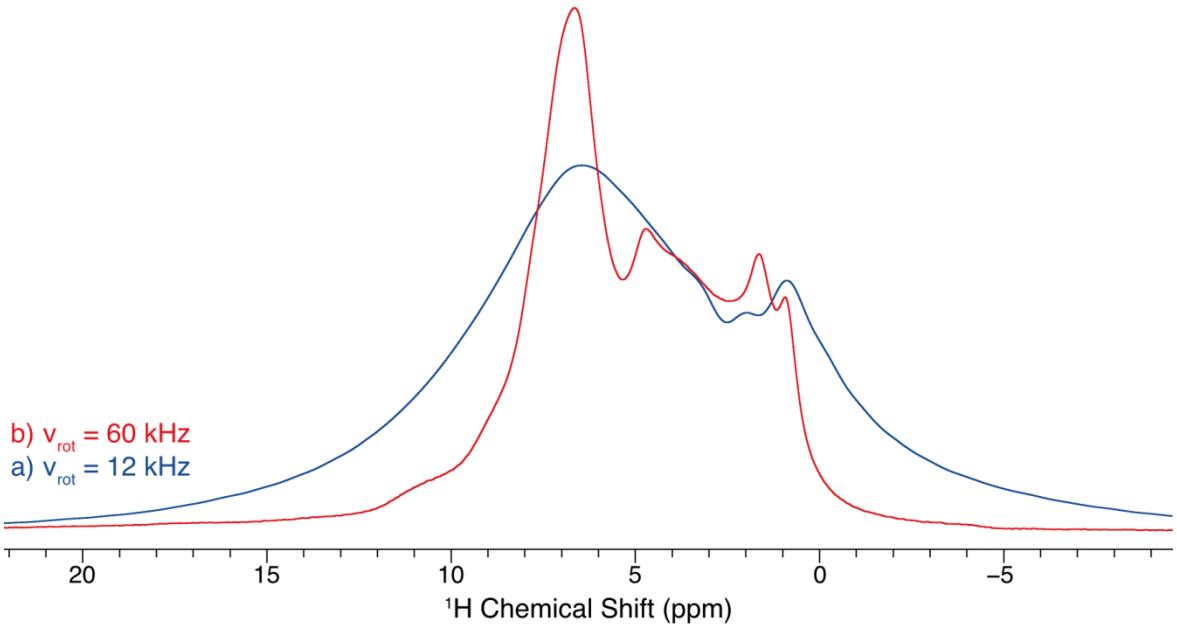

Figure S15. ^{1}H MAS spectra of **GNE-A^{AR}** at two different spinning rates a) ν_{rot} = 12 kHz, b) ν_{rot} = 60 kHz.

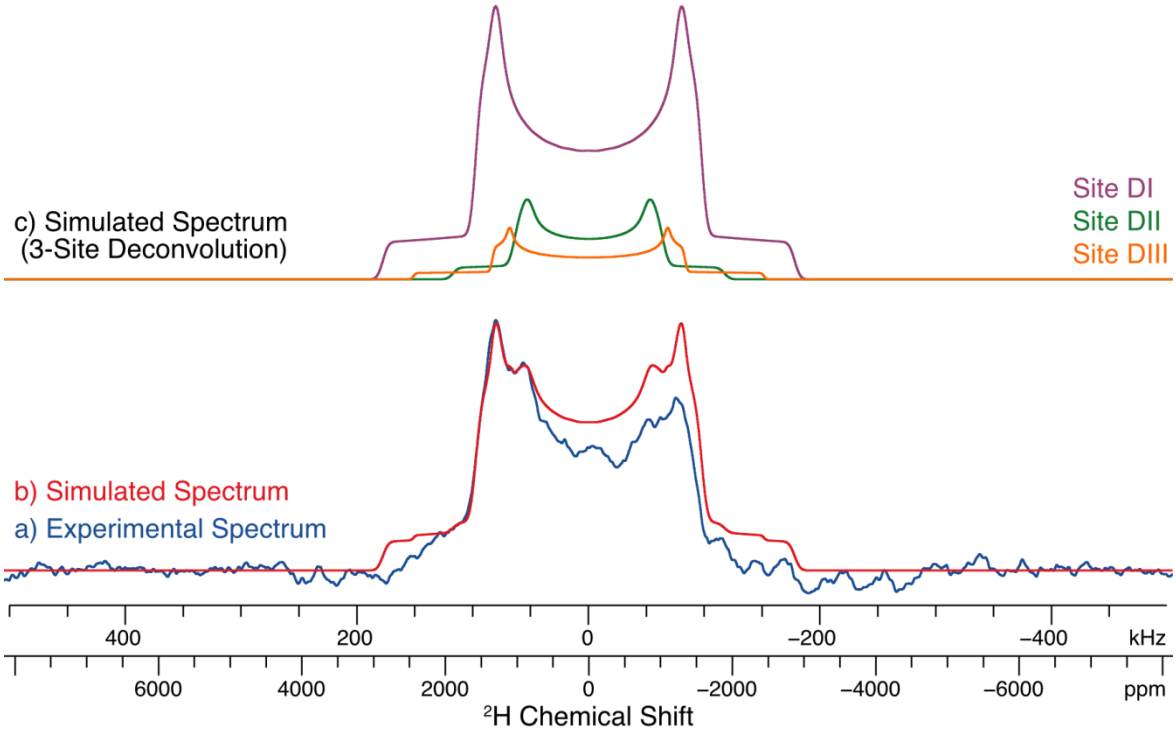

Figure S16. a) Experimental $^{2}H\{^{1}H\}$ quadrupolar-echo spectrum of **Rehydrate-D_2O** acquired at −125 ºC, b) analytical simulation without ^{2}H dynamics (*i.e.*, in the slow-motion limit) of the pattern constructed with the 3 subspectra shown in c).

Discussion of ^{1}H MAS/UFMAS and ^{2}H NMR Experiments (Figure S14 - Figure S16)

^{1}H MAS experiments conducted at ν_{rot} = 12 kHz (**Figure S14**) resulted in spectra with poor signal resolution. As such, these spectra did not reveal substantial differences between the samples, except for a variation in overall signal intensity (consistent with different water content) and an additional signal in the spectrum of **GNE-A^{LR}**, which may result from excess water molecules adsorbed on the surface of the API particles. ^{1}H UFMAS experiments conducted at ν_{rot} = 60 kHz resulted in spectra of higher resolution (**Figure S15**); however, due to the inability of the Bruker UFMAS probe to control sample temperature, it is possible that frictional heating results in partial or full dehydration of the material, rendering these spectra of limited use.

^{2}H NMR experiments yielded spectra (**Figure S16**) with poor S/N due to the low concentration of ^{2}H spins (even in samples prepared with pure D_2O, water accounts for a maximum of 3.5 wt-% of the sample when it is fully hydrated, and even less in the partially dehydrated materials). It is possible that the use of a variety of techniques (homonuclear decoupling, 2D-correlation experiments, higher magnetic fields, dynamic nuclear polarization, or a broader temperature range) may enable the acquisition of ^{1}H and ^{2}H spectra of these materials, but such experiments are beyond the scope of the current work.

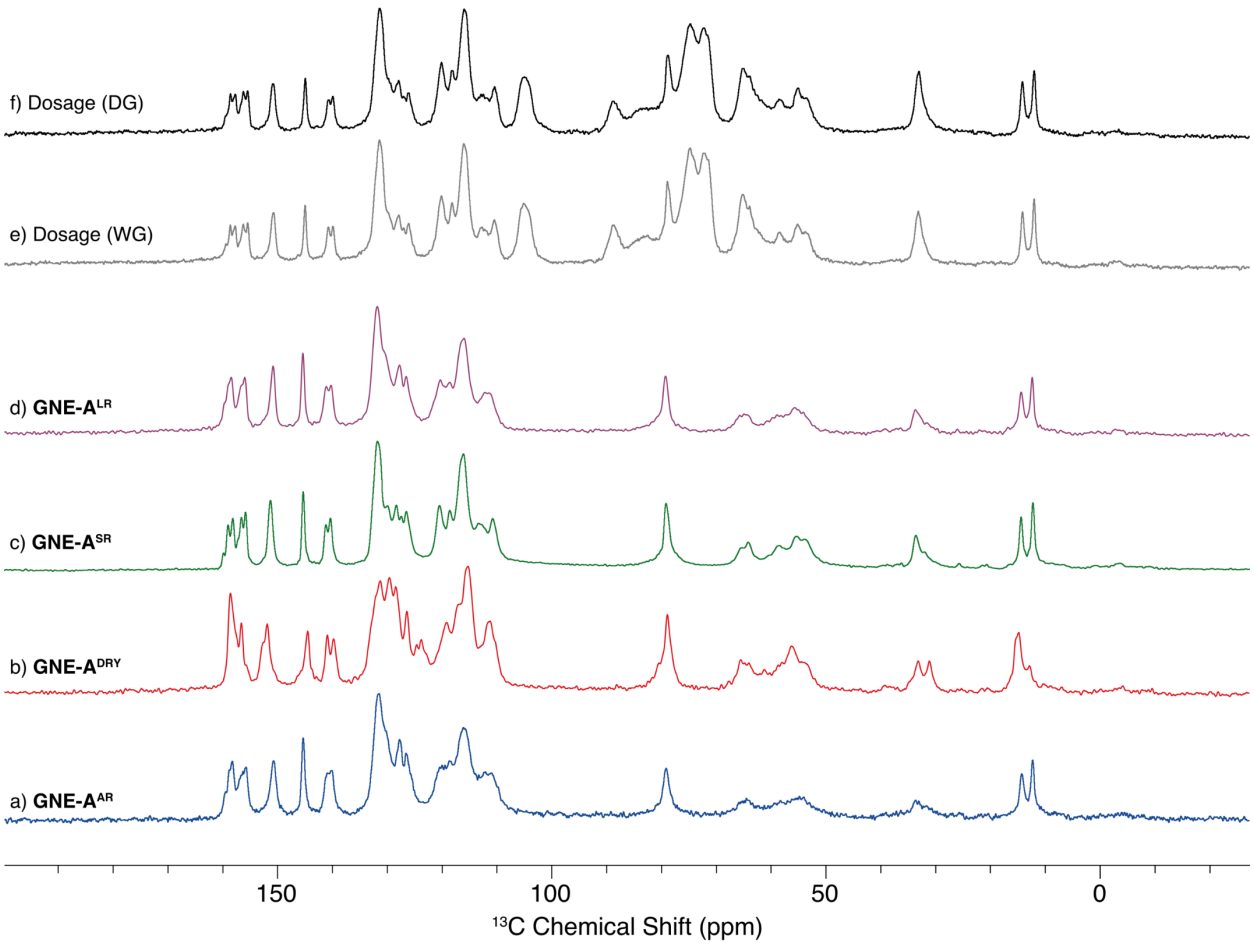

Figure S17. ^{1}H-^{13}C CP/MAS (ν_{rot} = 12 kHz) NMR spectra of the **GNE-A** samples prepared with different levels of hydration (a-d) and **GNE-**A dosage formulations processed using a) wet granulation or b) dry granulation. See text for details of the sample preparations. Spectra are scaled to have the same maximum intensity.

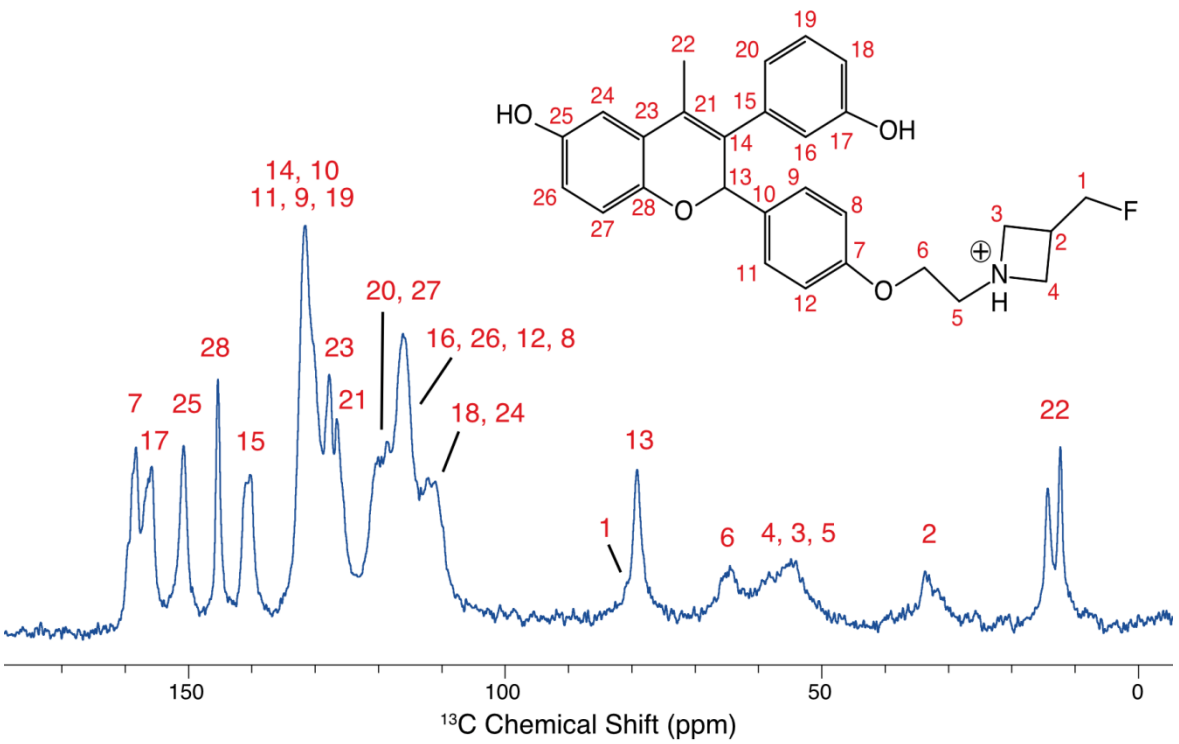

Figure S18. Peak assignments of the ^{1}H-^{13}C CP/MAS (ν_{rot} = 12 kHz) spectrum of the **GNE-A^{AR}** sample (the structure of **GNE-A** is shown in the inset).

Discussion of ^{13}C SSNMR Experiments (Figure S17 and Figure S18)

^{1}H-^{13}C CP/MAS spectra of the **GNE-A** samples are useful in supporting conclusions drawn from the ^{35}Cl SSNMR data discussed above. Due to their sensitivity to changes in the crystal structure, ^{13}C NMR spectra can provide information on the structural changes to the API molecules that occur as the result of water removal.[42–45] The ^{1}H-^{13}C CP/MAS (ν_{rot} = 12 kHz) spectra of the **GNE-A** samples are shown in **Figure S17**, and peak assignments based on solution NMR data are shown in **Figure S18**. Close examination of these spectra reveals that some of the sites in the molecular structure produce two or more resonances (*e.g.*, the peaks at *ca*. 12-15 ppm, and *ca.* 160 ppm). These additional resonances arise from magnetically-distinct sites associated with the two crystallographically distinct API molecules in the unit cell and/or from the presence of the two conformers.

Consistent with the ^{35}Cl NMR results, the largest differences in the ^{13}C NMR spectra of the four **GNE-A** samples are observed in those of **GNE-A^{AR}** and **GNE-A^{DRY}** (**Figure S17a** and **Figure S17b**, respectively). There are subtle differences in the shifts, especially in the region corresponding to carbons in the phenyl ring closest to the four-membered azetidine ring (*ca*. 125-135 ppm). These changes may indicate a slight change in the orientations of the ring to fill the void space produced by water removal. The shift of the ^{13}C peak corresponding to the carbon site that is closest to the water molecules (at 150.7 ppm in **Figure S17a**), which might be expected to be most affected by the removal of water, does not change significantly with heating. In fact, all of the chemical shifts from the hydrated and dehydrated materials are quite similar to each other, and as such, it would be difficult to discriminate between them in a ^{13}C SSNMR spectrum of a physical mixture of the hydrated and dehydrated materials. Nonetheless, ^{13}C SSNMR experiments are very useful for characterizing the bulk materials here, and are consistent with the results obtained from other nuclei and characterization methods.

The spectra of rehydrated samples (**Figure S17c** and **Figure S17d**) are nearly identical to that of **GNE-A^{AR}**, indicating that with rehydration, the carbon environments are "restored" to similar conditions as found in **GNE-A^{AR}**. This observation is also consistent with the ^{35}Cl SSNMR and variable RH PXRD results (*cf.* §3.6 and 3.7). Finally, the spectra of the formulated materials most closely resemble that of **GNE-A^{SR}** (*cf*. **Figure S17e, Figure S17f and Figure S17c**), however the presence of **GNE-A^{DRY}** cannot be ruled out due to the similarities of the spectra of **GNE-A^{DRY}** and the other hydrated materials discussed above.

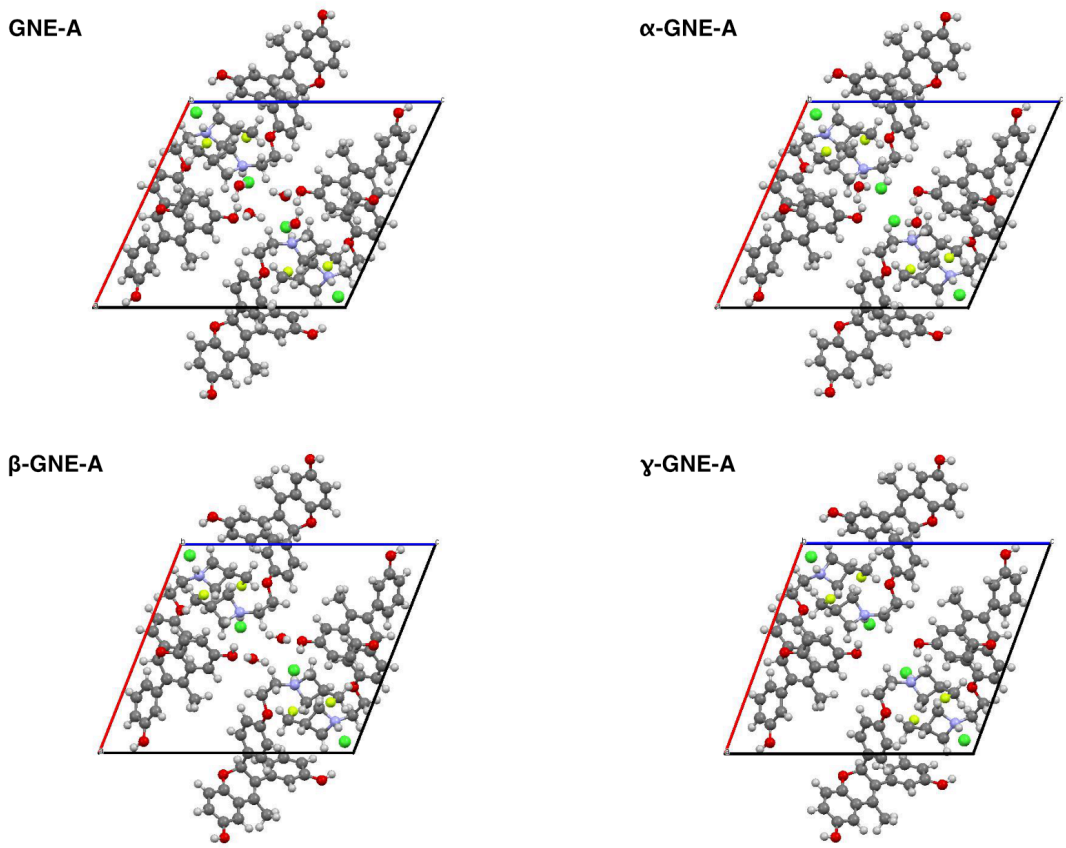

Figure S19. The crystal structures of GNE-A and the three model dehydrates. These structures were obtained following plane-wave DFT refinements of the crystal structure reported in this work, or on a version of the crystal structure with one or more water molecules removed. **Conformer A** is shown in all cases. The structures are viewed from the crystallographic *b*-axis.

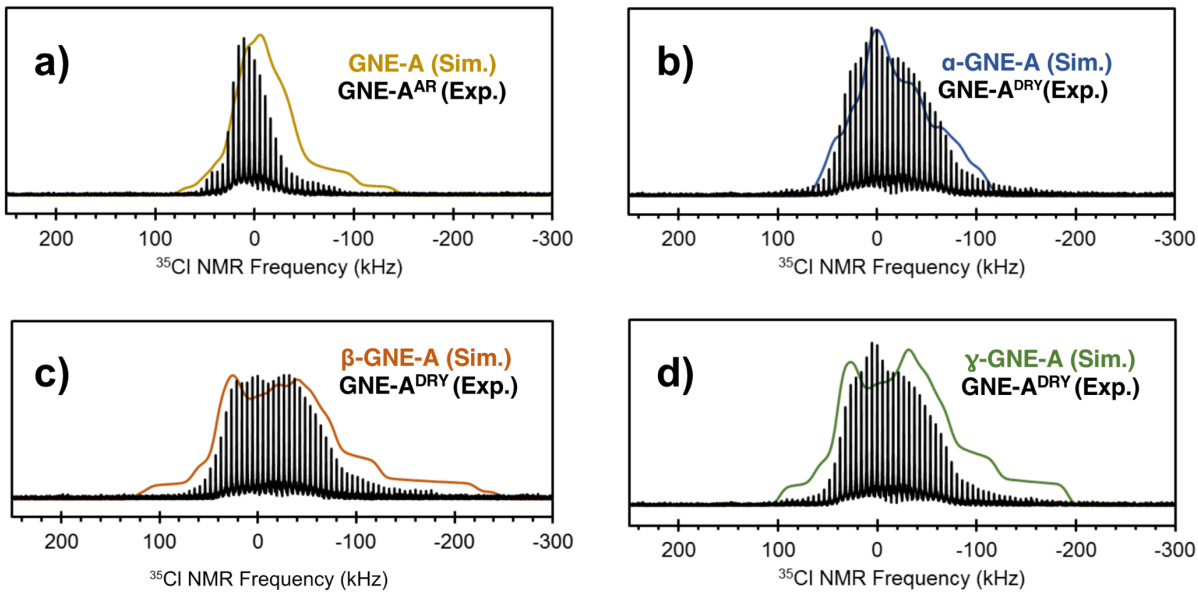

Figure S20. (a) Comparison of the simulated ^{35}Cl SSNMR pattern of **GNE-A** with an experimental ^{35}Cl spectrum of **GNE-A^{AR}**. (b-d) Comparison of the simulated ^{35}Cl SSNMR pattern of **α-GNE-A**, **β-GNE-A**, or **ɣ-GNE-A** with an experimental ^{35}Cl spectrum of **GNE-A^{DRY}**.

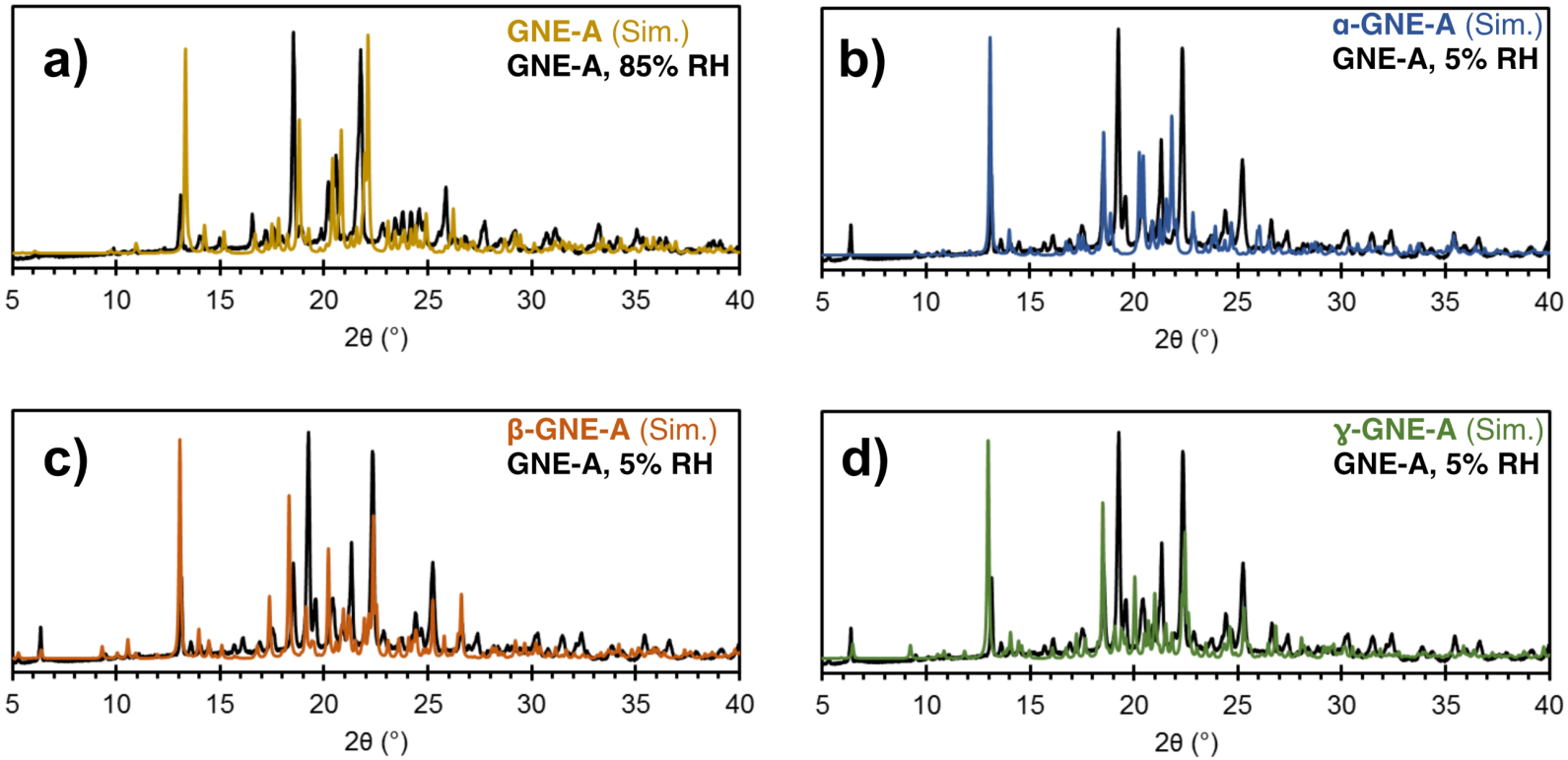

Figure S21. (a) Comparison of the simulated PXRD pattern of **GNE-A** with an experimental pattern of **GNE-A, 85%RH**. (b-d) Comparison of the simulated PXRD pattern of **α-GNE-A**, **β-GNE-A**, or **γ-GNE-A** with an experimental pattern of **GNE-A, 5%RH**.

References

(1) Hildebrand, M.; Hamaed, H.; Namespetra, A. M.; Donohue, J. M.; Fu, R.; Hung, I.; Gan, Z.; Schurko, R. W. 35 Cl solid-state NMR of HCl salts of active pharmaceutical ingredients: structural prediction, spectral fingerprinting and polymorph recognition. *CrystEngComm* **2014**, *16*, 7334.

(2) Harris, R. K.; Wasylishen, R. E.; Duer, M. J. *NMR Crystallography*, 1st ed.; Harris, R. K., Wasylishen, R. E., Duer, M. J., Eds.; John Wiley & Sons Ltd., 2009.

(3) Taulelle, F. Fundamental Principles of NMR Crystallography. *Encycl. Magn. Reson.* **2009**, 1–14.

(4) Martineau, C.; Senker, J.; Taulelle, F. NMR Crystallography. *Annu. Reports NMR Spectrosc.* **2014**, *82*, 1–57.

(5) Holmes, S. T.; Schurko, R. W. Refining Crystal Structures with Quadrupolar NMR and Dispersion-Corrected Density Functional Theory. *J. Phys. Chem. C* **2018**, *122*, 1809–1820.